RESEARCH PAPER

Molecular docking, molecular dynamics, and ADMET analysis of *Soymida febrifuga* phytoconstituent against Uropathogenic E. coli

Nita Kulkarni[1], Chaitanya Chilukuri[2], Sarika Sharma[3]*

[1]Department of Biotechnology, School of Bioengineering & Biosciences, Lovely Professional University, Phagwara–144411, Punjab, India.

[2]Independent Researcher, Hyderabad, Telangana, India.

[3]Department of Sponsored Research, Division of Research & Development, Lovely Professional University, Phagwara–144411, Punjab, India.

***Corresponding Author:**
Sarika Sharma
Department of Sponsored Research, Division of Research & Development, Lovely Professional University, Phagwara–144411, Punjab, India.
E-mail: Sarika.28186@lpu.co.in
Telephone: +91-9816535399

Abstract

Uropathogenic Escherichia coli (UPEC), a primary cause of urinary tract infections (UTIs),with increasing antimicrobial resistance necessitating the investigation of novel antibacterial agents. *Soymida febrifuga* contains bioactive phytoconstituents, including Luteolin-7-O-glucoside (L7G) with reported antimicrobial potential. This study computationally evaluated L7G against two previously proposed UPEC-associated protein targets, D-alanine–D-alanine ligase (Ddl) and AppA. Molecular docking followed by 100-ns molecular dynamics (MD) simulations was performed to assess predicted ligand- protein interactions and complex stability. MM-GBSA was used to estimate binding free energies, while SwissADME and pkCSM were employed for in silico pharmacokinetic and toxicity prediction. L7G showed predicted docking scores of −7.6 kcal/mol against Ddl and −8.9 kcal/mol against AppA. Both complexes showed generally stable interaction profiles during the 100-ns molecular dynamics simulations. MM-GBSA analysis showed a modestly more favourable estimated binding energy for AppA (−39.44 kcal/mol) than Ddl (−36.65 kcal/mol).

ADMET analysis indicated favourable solubility and low toxicity, despite low predicted gastrointestinal absorption. Overall, these findings provide preliminary, hypothesis-generating computational evidence for L7G interactions with the selected UPEC- associated targets; however, experimental validation, comparative benchmarking, replicate stimulations,and strain specific target validation are required to establish biological activity and target relevance.

Keywords: *Soymida febrifuga*, luteolin-7-O-glucoside, Molecular docking, Molecular dynamics, Uropathogenic Escherichia coli,

How to cite this article: Nita Kulkarni, Chaitanya Chilukuri, Sarika Sharma. Molecular docking, molecular dynamics, and ADMET analysis of Soymida febrifuga phytoconstituent against Uropathogenic E. coli. Int J Drug Deliv Technol. 2026;16(88s):803-814. DOI: 10.25258/ijddt.16.88s.82.

1. Introduction

Urinary tract infections (UTIs) are among the most prevalent bacterial infections affecting the human population, ranking second only to respiratory infections in both community and hospital settings. About 90% of UTIs are associated with Uropathogenic Escherichia coli (UPEC), bacterium responsible for both simple and complicated UTI cases, accounting for nearly 75% and 65% respectively[1]. Adhesion mechanisms, toxins production, iron absorption systems, and biofilm formation are characteristics of UPEC, an extraintestinal pathogenic *E. coli* (ExPEC) enabling survival and persistence outside the intestinal tract of the host and induce chronic infections[2- 4].

The emergence of Multidrug resistance (MDR) by UPEC strains has significantly reduced

effectiveness of conventional antibiotics [29-31]. This situation has prompted research into novel drugs and alternative therapies, focusing on plant-derived chemicals that may serve as potential antibacterial agents by utilizing various functional pathways and preventing development of resistance[5, 6, 32].

Extracts of *Soymida febrifuga* (Indian Redwood), an Ayurvedic medicinal herb, have demonstrated antibacterial activity against UPEC, especially those derived from leaves, roots, and bark[7-10].Luteolin-7-O-glucoside (cynaroside), a phytoconstituent reported from S. febrifuga, has demonstrated antimicrobial activity against Gram-negative bacteria, including E. coli[11, 12].

Previous Computational studies have proposed D-alanine-D-alanine ligase (Ddl) and AppA as potential UPEC- associated protein targets involved in distinct bacterial processes. Ddl is involved in peptidoglycan biosynthesis, making it a biologically relevant protein for target based antibacterial investigation. Previous experimental evidence has shown that the flavonoids quercetin and apigenin can inhibit Ddl, supporting the investigation of flavonoid-derived compounds against this target[13-16, 37].

In silico approaches such as molecular docking, molecular dynamics simulations, and ADMET prediction are widely used in early stage drug discovery to investigate predicted protein- ligand interactions and pharmacokinetic properties while reducing the resources required for preliminary screening.

The present study computationally evaluates luteolin-7-o-glucoside (L7G), a phytoconsituent of *soymida febrifuga*, for its anticipated interactions with two previously proposed UPEC-associated protein targets, Ddl and AppA, using molecular docking, molecular dynamics, MM-GBSA and ADMET analyses. The objective was to characterize the predicted interaction modes, dynamic behaviour and binding energetics of L7G with these selected targets and generate hypotheses for further investigation. As a single-ligand computational study without experimental validation or reference comparators, the findings provide preliminary evidence rather than establishing antibacterial efficacy or target selectivity.

2. Materials and Methods

2.1 Ligand Preparation

Luteolin-7-O-glucoside (cynaroside, L7G), a flavonoid glycoside, was selected based on its reported occurrence in *Soymida febrifuga* and previously reported antimicrobial potential. Its canonical SMILES was retrieved from PubChem (CID: 45933934) and converted into a 3D structure using Open Babel v3.1.1. The ligand was energy-minimized and saved in PDBQT format after Gasteiger charge addition via AutoDockTools v1.5.7.

2.2 Target protein preparation

Previous computational work proposed Ddl and AppA as potential UPEC- associated protein targets. D-alanine–D-alanine ligase (Ddl; PDB ID: 4C5B) is a cytoplasmic enzyme that catalyzes the ATP – dependent formation of D-alanyl–D-alanine, an important step in peptidoglycan biosynthesis[38].

AppA (PDB ID:7Z1J) is an E.coli phytase belonging to the histidine phosphatase family and is involved in phosphate metabolism[16].The crystal structure was used as a representative protein structure for computational target investigation. Crystal structures were retrieved from Protein Data Bank, adding polar hydrogen atoms, and assigning Kollman partial charges; crystallographic water molecules and non-essential heteroatoms were removed prior to saving proteins in PDBQT format for docking simulations[17, 18]. Ddl (PDB ID: 4C5B) and AppA (PDB ID: 7Z1J) were selected as representative E. coli protein structures for the computational analysis based on their previously proposed relevance as potential UPEC-associated targets. High-affinity sites were mapped by blind docking (Section 2.3); the highest-scoring locus underwent targeted redocking and served as the initial configuration for MD simulations.

2.3 Molecular Docking

Molecular docking of L7G against *E. coli* Ddl (PDB ID: 4C5B) and AppA (PDB ID: 7Z1J) was executed in AutoDock Vina v1.2.2. The PDB-derived protein structures were prepared by removing non-essential heteroatoms and adding polar hydrogen atoms and Kollman partial charges using AutoDock v1.5.7. L7G was parameterized through energy-minimization, Gasteiger charge computation, and PDBQT formatting. Docking was conducted using two-stage protocol: blind docking to identify potential binding sites, followed by focused docking on top-ranked pocket. Grid parameters were set for (Ddl: x = 0.79, y = 21.77, z = 63.49; 48 × 56 × 46 Å; AppA: x = −25.52, y = −1.18, z = −14.88; 40 × 40 × 40 Å).

Docking was performed with an exhaustiveness of 8, generating up to 10 poses per run. Predicted docking scores were obtained using the Vina scoring function, and top poses were selected based on lowest energy and consistency. Interactions were analyzed using PyMOL to evaluate hydrogen bonding, hydrophobic contacts, and proximity to functionally relevant residues, and best ligand–

protein complexes were used for molecular dynamics simulations to assess binding stability.

2.4 Molecular Dynamics Simulations

Molecular dynamics (MD) simulations were performed using Desmond 2020.1 (Schrodinger, LLC) for Ddl–L7G (4C5B) and AppA–L7G (7Z1J) complexes. OPLS-2005 force field was applied, and systems were solvated in an explicit TIP3P water model within a 10 Å buffer[19-22]. Counter ions (Na^+) were added to neutralize the system, with additional NaCl included to mimic physiological conditions. Following energy minimization, equilibration was conducted under NVT (10 ns) and NPT (12 ns) ensembles using Nosé–Hoover chain coupling scheme and Martyna Tuckerman–Klein barostat[23, 24]. A 2 fs integration step was applied, and long-range electrostatic interactions were treated using particle-mesh Ewald (PME) method with a 9 Å cutoff [25]. Production simulations were performed for 100 ns under periodic boundary conditions. Protein and complex dynamic behavior was evaluated using RMSD, RMSF, radius of gyration (Rg), solvent-accessible surface area (SASA), and hydrogen bond and salt bridge analyses[26]. A single 100-ns production trajectory was analyzed for each protein–ligand complex, with comparative analyses interpreted as trajectory-specific computational observations.

2.5 Pharmacokinetics and ADMET Prediction

Physicochemical properties and pharmacokinetic parameters of luteolin-7-O-glucoside were predicted using SwissADME[27]. Additional ADMET properties, including absorption, distribution, metabolism, excretion, and toxicity endpoints, were evaluated using pkCSM based on canonical SMILES input[28]. Predicted parameters included %HIA, Caco-2 permeability, volume of distribution Vdss, clearance, CYP interactions, and toxicity profiles. Results are summarized in Table 2.

2.6 Binding free energy analysis

Binding free energy of protein–ligand complexes was estimated using Molecular Mechanics–Generalized Born Surface Area (MM-GBSA) method implemented in Prime (Schrödinger, LLC) via thermal_mmgbsa.py script. Analysis was performed on final 50 frames of molecular dynamics trajectories. The total binding free energy (ΔG_bind, $kcal \cdot mol^{-1}$) was derived from contributions including electrostatic interactions, van der Waals forces, lipophilic, hydrogen bonding, and solvation energies.

Binding free energy ($\Delta Gbind$) was computed using the equation:

$$\Delta Gbind = \Delta GMM + \Delta Gsolv - \Delta GSA$$

Here, ΔG_MM represents molecular mechanics energy difference between complex and unbound components, ΔG_solv denotes differential solvation energy, and ΔG_SA corresponds to surface area energy contribution.

The MM-GBSA values were used as comparative computational estimates rather than experimentally measured binding affinities. The relative differences between the complexes were considered within the present computational framework, and future studies incorporating independent simulation replicates and experimental validation may further clarify the binding energetics and target relevance of L7G.

3. Results

3.1 Molecular Docking Results

Three dimensional structures of Ddl and AppA are shown in Fig 1. Molecular docking of luteolin-7-O-glucoside (cynaroside, L7G) against *E. coli*, D-alanine–D-alanine ligase (Ddl, PDB ID: 4C5B) and AppA (PDB ID: 7Z1J) yielded favorable predicted docking poses for both selected protein structures (Table 1). Highest affinity pose of L7G in Ddl showed a binding energy of -7.6 $kcal \cdot mol^{-1}$, with additional poses ranging from -7.4 and -7.3 $kcal \cdot mol^{-1}$.

In comparison, a more negative predicted docking score was obtained for AppA than for Ddl under the docking conditions used, where top-ranked pose scoring -8.9 $kcal \cdot mol^{-1}$, followed by poses at -8.8 and -8.7 $kcal \cdot mol^{-1}$. The relatively close clustering of the AppA docking poses (RMSD 1–3 Å) indicates consistency among the predicted poses within the selected docking protocol (Fig 2 and 3). Overall, L7G demonstrated favourable predicted interactions with both targets, with AppA showing a comparatively more favourable docking Score than Ddl (Figs. 4 and 5), consistent with dynamic stability observed in molecular dynamics simulations.

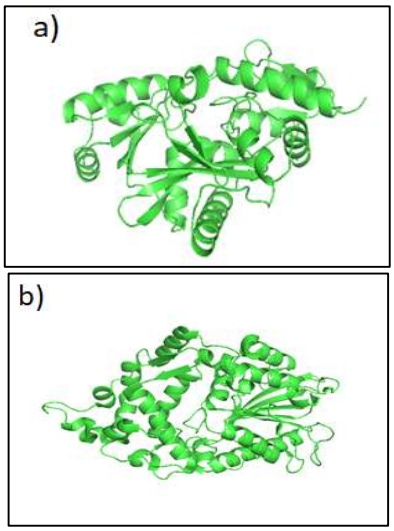


Figure 1. Overall three-dimensional structure of *E. coli* a) D-alanine–D-alanine ligase (Ddl) and b) AppA. Protein is displayed as a green representation showing α-helices and β-strands that form active-site cleft.

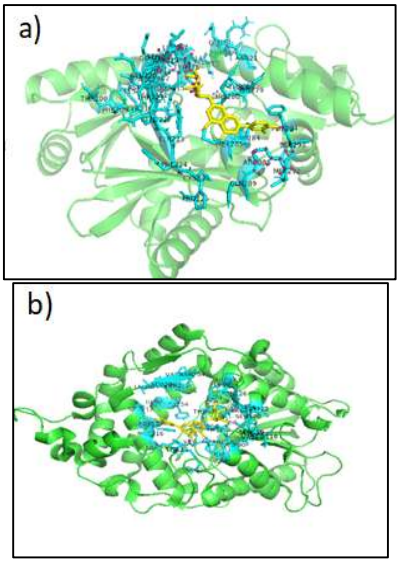


Figure2. Binding pocket of a) Ddl and b) AppA showing the luteolin-7-O-glucoside (L7G) ligand (yellow sticks) docked within the pre dicted binding site of both the targets. The surrounding amino acid residues (cyan sticks) form hydrogen bonds and hydrophobic contacts stabilizing the complex

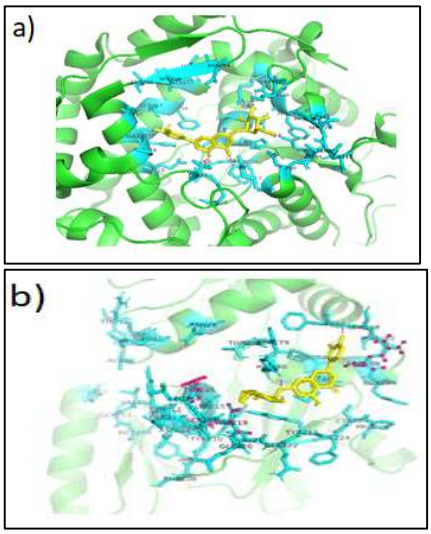


Figure 3. Detailed visualization of binding pocket of a) Ddl and b) AppA showing hydrogen-bond distances (in Å) and orientation of residues forming polar and hydrophobic contacts with the ligand. Cyan residues denote the active-site environment, and the ligand is displayed in yellow.

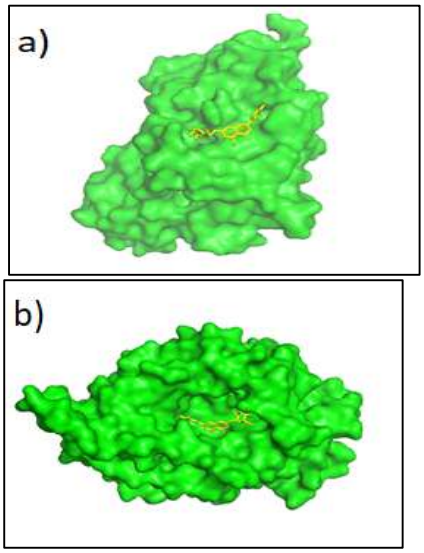


Figure 4. Solvent-accessible surface representation of a) Ddl and b) AppA (green) showing the location of L7G (yellow sticks) bound in the surface cavity. The surface model reveals the extent of the pocket and ligand burial, illustrating how L7G fits into the accessible groove of the enzyme.

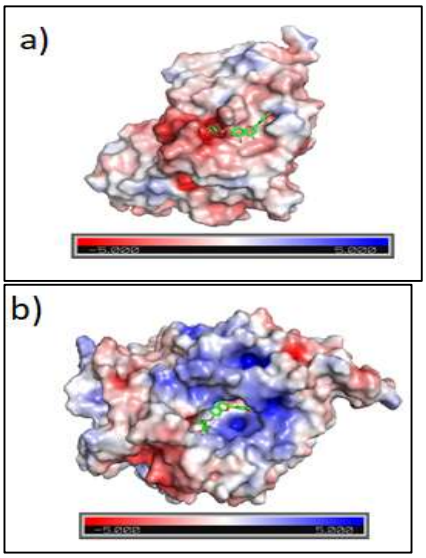


Figure 5. Electrostatic potential surface of a) Ddl and b) AppA computed using APBS plugin. The surface is colored from red (negative potential) to blue (positive potential), with neutral regions shown in white.

Table 1: Binding Affinities of Luteolin–7-O–glucoside to Ddl and AppA

Mode	Affinity (Kcal/mol) Ddl	Affinity (Kcal/mol) AppA
1	-7.6	-8.9
2	-7.4	-8.8
3	-7.3	-8.7
4	-7.2	-8.6
5	-7.2	-8.6
6	-7.2	-8.5
7	-7.1	-8.4
8	-7.0	-8.4
9	-7.0	-8.3

3.2 Pharmacokinetics and ADMET Predictions

Swiss ADME predicted that luteolin-7-O-glucoside (L7G) has a molecular weight of 448.38 g/mol, a TPSA of 190 Å², 7 hydrogen bond donors and 11 acceptors, and a consensus LogP of 0.2. pkCSM estimated intestinal absorption at 37.6%, Caco-2 permeability of ~1.8×10^{-6} cm/s, and a volume of distribution of 7.6 L/kg (logVdss 0.884) with a fraction unbound of 0.22. No CYP liabilities were flagged, clearance was modest (~3.0 mL/min/kg), and toxicity endpoints were negative (Table 2).

The predicted ADMET profile indicated that the high polarity of L7G may influence its systemic exposure, while its predicted solubility and favorable toxicity profile support its further investigation as a natural-product scaffold. The predicted pharmacokinetic characteristics provide insights into the absorption, distribution, metabolism, and potential biological behavior of L7G.

Table 2. Predicted physicochemical, pharmacokinetic, and toxicity properties of luteolin-7-O-glucoside (L7G)

Category	Parameter	Predicted Value	Unit / Interpretation	Prediction Source
Physicochemical Properties	Molecular Formula	C21H20O11	—	SwissADME
	Molecular Weight	448.38	g·mol⁻¹	SwissADME
	TPSA	190.28	Å² → high polarity = low permeability	SwissADME
	H-bond Donors / Acceptors	7 / 11	Slightly above Lipinski limits	SwissADME
	Rotatable Bonds	4	—	SwissADME
	Consensus LogP	0.19	Hydrophilic compound	SwissADME
	Water Solubility (Log S, ESOL/Ali/SILICOS-IT)	-3.65 / -5.06 / -2.10	Soluble to moderately soluble	SwissADME
Pharmacokinetics	GI Absorption	Low	Limited oral bioavailability	SwissADME
	BBB Permeant	No	Non-permeant	SwissADME
	P-gp Substrate	Yes	Possible efflux liability	SwissADME / pkCSM
	Bioavailability Score	0.17	Low oral bioavailability	SwissADME
	Caco-2 Permeability	0.248	log Papp (10^{-6} cm/s) → low permeability	pkCSM
	Human Intestinal Absorption (%HIA)	37.56	Poor absorption	pkCSM

	VDss (Human)	0.884	log L/kg ≈ 7.6 L/kg→ moderate distribution	pkCSM
	Fraction Unbound (fu)	0.224	Moderate protein binding	pkCSM
	Total Clearance	0.478	log mL·min^{-1}·kg^{-1} ≈3.0mL/min/kg	pkCSM
Toxicity	AMES Mutagenicity	No	Non-mutagenic	pkCSM
	hERG I / II Inhibition	No / No	Non-cardiotoxic	pkCSM
	Hepatotoxicity	No	Safe liver profile	pkCSM
	Skin Sensitization	No	Non-sensitizing	pkCSM
	Oral Rat Acute Toxicity (LD50)	2.547	mol/kg → moderate toxicity	pkCSM
	Oral Rat Chronic Toxicity (LOAEL)	4.279	log mg/kg_bw/day ≈19 mg/kg/day	pkCSM

3.3 Molecular Dynamics Simulation

MD simulations were performed to evaluate stability and convergence of 4C5B_ligand (Ddl) and of 7Z1J_ligand (AppA) complexes. Fig 6(a) represents RSMD profile of 4C5B_ligand (Ddl), showed a rapid increase during initial equilibration phase (0-5) ns, followed by stabilization at an average of 1.74 Å. Minor fluctuations at 40 ns and 85–90 ns, remained within an acceptable range (<3 Å), indicating a stable binding orientation throughout 100 ns simulation. Fig 6(b) represents RMSD profile of 7Z1J_ligand (AppA) increased gradually over first 20 ns and stabilized within 1.5-2.0 Å, maintaining an average of 1.62 Å with minor fluctuations beyond 60 ns, suggesting stable ligand binding. Fig 7(a) represents RMSF analysis of 4C5B_ligand (Ddl) revealed higher flexibility at terminal regions, with peaks up to ~5 Å at N-terminus, while most residues showed minimal fluctuations (average ~0.94 Å), indicating overall stability. Similarly, 7Z1J_ligand (AppA) exhibited fluctuations below 1.5 Å for most residues, except residue 180 (~ 3 Å), suggesting localized flexibility associated with a loop region. Rg analysis of 4C5B_ligand (Ddl) in Fig 8(a) indicates structural compactness, with Rg values consistently between 4.71 Å and 5.43 Å. Fig 8(b) illustrates Rg analysis of 7Z1J–ligand (AppA), showing values between 4.59 Å and 5.42 Å, with minor dips at 20 ns and 50 ns before stability was regained. Fig 9(a) illustrates the hydrogen bond analysis of 4C5B_ligand (Ddl) complex, which exhibited stability with a consistent formation of 0-8 hydrogen bonds, stabilizing around 2-3 after initial peaks. Fig 9(b) shows 7Z1J_ligand (AppA) complex maintaining an average of 1-7 hydrogen bonds over the trajectory, with occasional peaks up to 12. The interaction analysis showed differences in the hydrogen-bond and residue-contact profiles between the two complexes. Fig. 10 shows the solvent-accessible surface area (SASA) profiles of the Ddl–L7G and AppA–L7G complexes throughout the 100-ns trajectories. The observed SASA profiles provide information on changes in solvent exposure and conformational behavior within the modeled complexes. Because unbound/apo protein simulations were not performed, the present analysis does not permit direct comparison of ligand-bound and unbound states or conclusions regarding ligand-induced receptor stabilization.

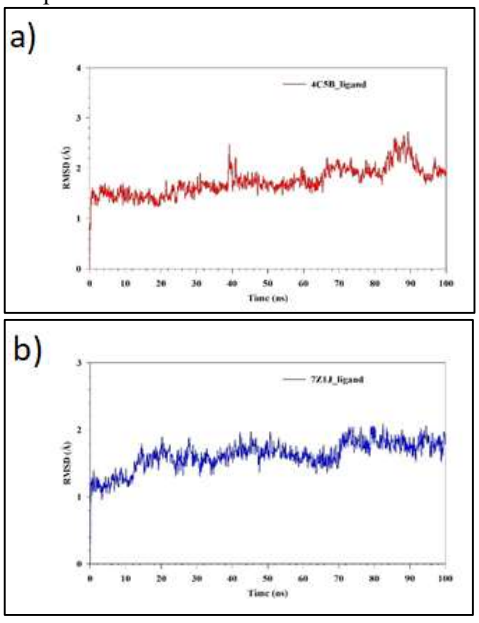


Figure 6. Molecular Dynamics simulation of 100 ns trajectories of **a)** RMSD of Cαbackbone of Ddl (4C5B_ligand)**b)**RMSD of Cα backbone of AppA (7Z1J_ligand).

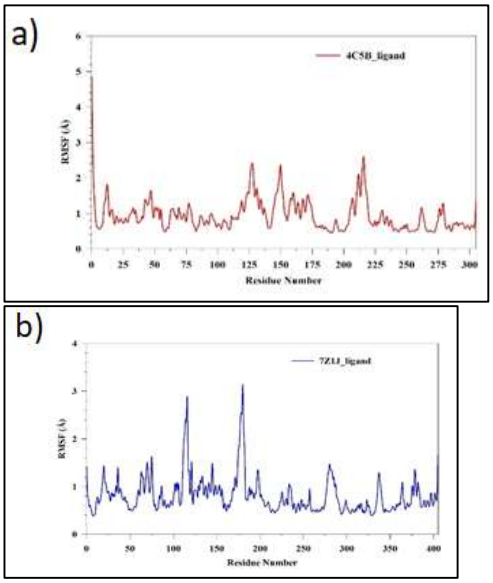


Figure 7: MD simulation analysis of 100 ns trajectories of **a)** RMSF of Cα backbone of Ddl (4C5B_ligand) b**)** RMSF of Cα backbone of AppA (7Z1J_ligand).

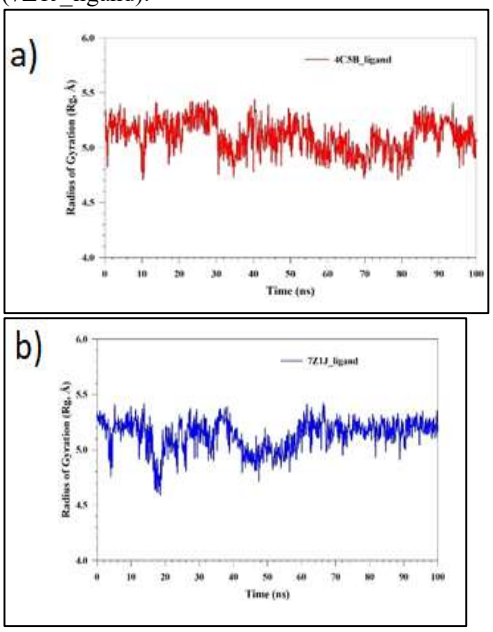


Figure 8: MD simulation analysis of 100 ns trajectories of **a)** Radius of gyration (Rg) of Cα backbone of Ddl (4C5B_ligand) **b)** Radius of gyration (Rg) of Cα backbone of AppA (7Z1J_ligand).

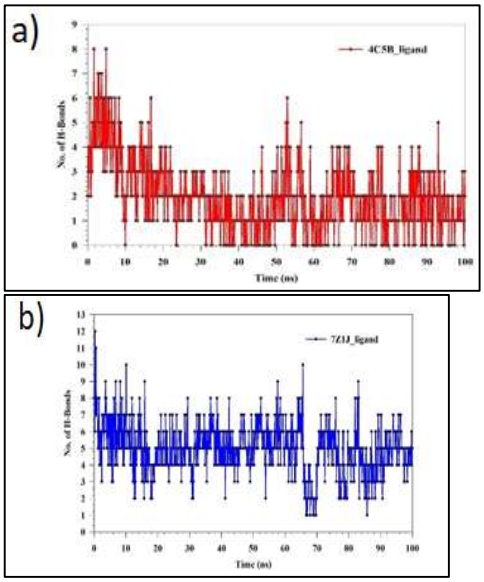


Figure 9: MD simulation analysis of 100 ns trajectories of **a)** Formation of hydrogen bonds in Ddl (4C5B_ligand) **b)** Formation of hydrogen bonds in AppA (7Z1J_ligand).

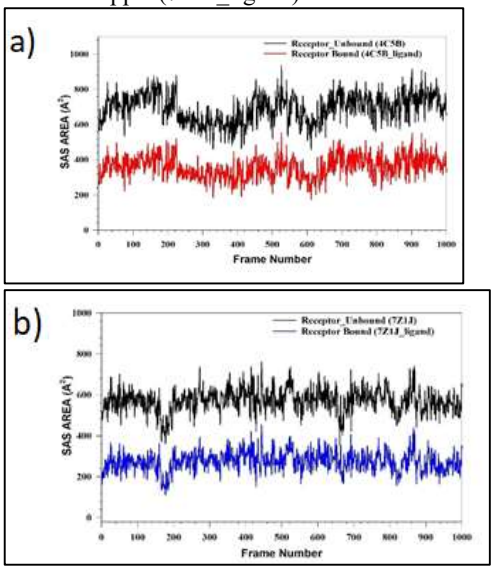


Figure 10: MD simulation analysis of 1000 Frame work of Solvent accessible surface area of a**)** Ddl (4C5B_ligand) **b)** AppA **(**7Z1J_ligand).

Protein-ligand interactions were assessed through 100 ns simulation studies. Interaction fractions were analyzed using stacked colored bars, indicating significant interactions for the complexes 4C5B_ligand and 7Z1J_ligand. In 4C5B_ligand, key interacting residues included ASP219 (50%), TYR216 (12%), and ARG288 (15%) for hydrogen bonds, while TYR210 (26%), HIS280 (26%), and TYR223 (39%) formed water bridges and ionic interactions. In 7Z1J_ligand, major residues were ASP122 (70%), ASN126 (44%), and others, primarily interacting via water bridges and hydrogen bonds, with HIS303 and

ARG92 showing hydrophobic and ionic interactions.

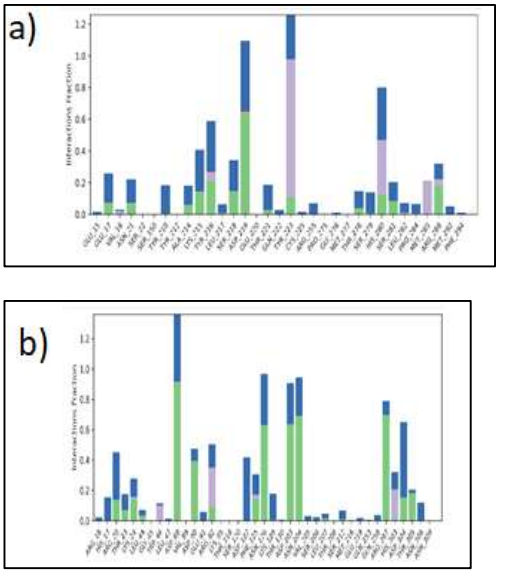


Figure 11: Bar graph of Protein-ligand contacts of **a)** Ddl (4C5B_ligand) **b)** AppA (7Z1J_ligand) showing interaction fraction of amino acid residues over period of simulation.

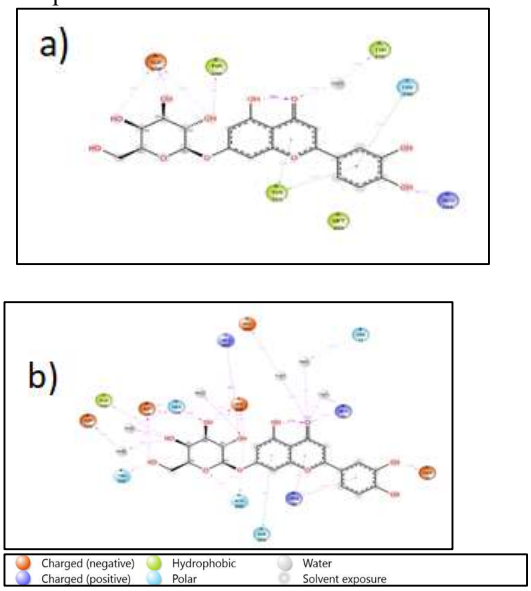


Figure 12: Protein-ligand percent interactions of **a)** Ddl (4C5B_ligand) **b)** AppA (7Z1J_ligand) over the period of simulation.

3.4 Molecular Mechanics Generalized Born Surface Area (MM-GBSA) calculations

Utilizing MD simulation trajectory, binding free energy along with other contributing energy in form of MM-GBSA is determined for 4C5B_ligand (Ddl), 7Z1J_ligand (AppA) complexes. **Table 3** represents the estimated MM-GBSA binding free energy for 7Z1J–L7G (AppA) was more favorable (ΔGbind = −39.44 kcal/mol) than that estimated for 4C5B–L7G (Ddl) (ΔGbind = −36.65 kcal/mol). Both complexes showed strong electrostatics (slightly higher in 7Z1J_ligand, AppA); van der Waals were stronger in 4C5B_ligand (Ddl), while hydrogen bonding was stronger in 7Z1J_ligand (AppA), indicating differences in the estimated interaction energetics between the two complexes. Lipophilic stabilization was greater in 4C5B_ligand (Ddl) than in 7Z1J_ligand (AppA). This indicates that 4C5B_ligand (Ddl) likely interacts more via nonpolar contacts, whereas 7Z1J_ligand (AppA) relies more on polar and H-bonding interactions. 7Z1J_ligand (AppA), showed slightly higher unfavourable covalent energy and stronger packing stabilization. Overall, the calculated energy components indicate distinct interaction profiles, with relatively greater electrostatic and hydrogen-bonding contributions for AppA–L7G and relatively greater lipophilic and van der Waals contributions for Ddl–L7G.

Table 3: Binding free energy components for the 4C5B_ligand (Ddl), 7Z1J_ligand (AppA) calculated by MM-GBSA.

Energies (kcal/mol)	**4C5B_ligand**	**7Z1J_ligand**
ΔG_{bind}	-36.65±2.86	-39.44±2.59
ΔG_{bind}Coulomb	-28.67±3.43	-31.71±4.70
ΔG_{bind}Covalent	2.10±0.79	2.76±1.59
ΔG_{bind}Hbond	-2.13±0.38	-4.30±0.34
ΔG_{bind}Lipo	-9.32±0.53	-6.19±0.30
ΔG_{bind}Packing	-2.81±0.6	-3.44±0.68
ΔG_{bind}SolvGB	36.94±3.76	32.81±2.33
ΔG_{bind}vdW	-32.76±1.82	-29.38±1.38

4. Discussion

The present study provides a focused computational analysis of L7G against two previously proposed UPEC-associated protein targets, Ddl and AppA, which are involved in distinct bacterial processes[13–16]. In this context, plant-derived flavonoids such as L7G may provide chemical diversity for early-stage drug discovery[11, 12]. Molecular docking is widely used in structure-based drug discovery to investigate potential protein–ligand interactions, while molecular dynamics simulations can provide information on the dynamic behavior of protein–ligand complexes[33, 36]. The present findings are computational and should be considered preliminary and hypothesis-generating, with further experimental validation required.

Distinct interaction patterns were observed for L7G across the selected Ddl and AppA targets, with AppA exhibiting a more favourable predicted

docking score than Ddl. These differences may be associated with variations in the topology and physicochemical characteristics of the predicted binding pockets, including hydrogen-bonding, electrostatic, van der Waals, and other non-covalent interactions[33].The MD simulations further showed that both modelled complexes maintained generally stable trajectory profiles over the 100-ns simulation period, supporting the persistence of L7G within the predicted binding regions under the simulated conditions[36].Collectively these findings provide structural and dynamic insights into the predicted interactions of L7G with the selected targets. Future biochemical and experimental studies may further characterize the binding affinity, inhibitory activity, and biological relevance of these predicted interactions.

The MM-GBSA analysis provided additional insight into the energetic basis of the predicted L7G interactions with Ddl and AppA. The more favorable estimated ΔG_bind for AppA (−39.44 kcal/mol) compared with Ddl (−36.65 kcal/mol) may reflect differences in the physicochemical environments of their respective binding pockets. In particular, the greater electrostatic and hydrogen-bonding contributions observed for AppA suggest that polar interactions may contribute substantially to L7G stabilization in this complex, whereas the relatively stronger van der Waals and lipophilic contributions observed for Ddl indicate a comparatively greater contribution from nonpolar interactions. Thus, L7G appears to engage the two modeled proteins through distinct combinations of intermolecular interactions. Future studies using independent simulation replicates, suitable reference ligands, and biochemical assays could further define the robustness of these energetic differences and their biological relevance[36].

From a pharmacokinetic perspective, ADMET predictions indicated that L7G exhibits favorable predicted toxicity-related properties, including no major toxicity liabilities predicted by the computational models used. Its high polarity and limited predicted gastrointestinal absorption may restrict systemic bioavailability[27, 28]. Future pharmacokinetic and biological studies may further characterize the absorption, distribution, metabolism, and safety-related properties of L7G[27, 28].

Overall, the study provides preliminary computational evidence supporting the potential interaction of L7G with the selected UPEC-associated protein targets. The integrated docking, molecular dynamics, and MM-GBSA analyses provide complementary structural and energetic insights into the predicted L7G–Ddl and L7G–AppA complexes[33,36]. The findings provide an initial assessment of L7G as a natural-product scaffold and establish a basis for further investigation of its target-associated interactions. Future studies incorporating broader virtual screening, structurally related flavonoids, suitable reference compounds, structure–activity relationship analyses, and experimental validation could further contextualize the predicted interactions and clarify the biological relevance and antibacterial potential of L7G.

The focused design of the present computational analysis provides several opportunities for further investigation. The selected PDB structures (4C5B and 7Z1J) represent E. coli protein structures, and future sequence-based studies could further establish their correspondence with the respective proteins in MDR-UPEC clinical isolates. The selected PDB structures (4C5B and 7Z1J) represent E. coli protein structures, and future sequence-based studies could further establish their correspondence with the respective proteins in MDR-UPEC clinical isolates. This consideration is particularly relevant to Ddl because E. coli contains two D-alanine–D-alanine ligases, DdlA and DdlB[39], making target-specific sequence characterization an important area for future investigation. Future computational studies incorporating independent MD replicates and broader comparative analyses could provide greater confidence in the reproducibility of trajectory behavior and the robustness of the MM-GBSA estimates.

Further experimental investigations, including enzyme-inhibition assays, MIC/MBC determination, UPEC growth and biofilm assays, and appropriate infection models, could evaluate whether the predicted interactions translate into measurable antibacterial activity[35, 36]. Broader virtual screening, structurally related flavonoids, validated reference compounds, and structure–activity relationship analyses could also provide additional context for the target-associated activity of L7G. Together, these computational findings provide a basis for further investigation of L7G as a natural-product scaffold against selected UPEC-associated targets. Future biochemical, microbiological, pharmacokinetic, and translational studies may further clarify the biological relevance and antibacterial potential of L7G[35, 36].

5. Study Limitations and Future Perspectives

Several considerations should be taken into account when interpreting the present findings. The study evaluated a single ligand, L7G, against two selected UPEC-associated targets, Ddl and AppA, providing a focused computational assessment. Future studies could extend this analysis through broader virtual screening, analogue comparison, structure–activity relationship (SAR) analysis, and benchmarking with validated Ddl inhibitors, AppA ligands, antibiotics, or structurally related flavonoids. Sequence-based characterization of the selected PDB structures against clinical MDR-UPEC isolates and independent MD trajectories for each complex could further strengthen target-

specific and trajectory-based interpretation. Additional comparative analyses could further clarify the relative MM-GBSA profiles and target-associated interactions of L7G, while enzyme-inhibition assays, MIC/MBC testing, UPEC growth and biofilm studies, and appropriate infection models could further evaluate its biological relevance and antibacterial potential

6. Conclusion

This study provides preliminary computational evidence supporting the potential interaction of luteolin-7-O-glucoside (L7G) with the selected UPEC-associated proteins Ddl and AppA. The integrated docking, molecular dynamics, and MM-GBSA analyses provide complementary structural and energetic insights into the predicted L7G–Ddl and L7G–AppA complexes, with AppA exhibiting a more favorable estimated binding energy under the applied computational conditions. ADMET analysis indicated favourable predicted toxicity-related characteristics alongside limited predicted gastrointestinal absorption, providing useful insights into the pharmacokinetic profile of L7G. Future studies incorporating broader comparative screening, suitable reference compounds, independent MD replicates, sequence-based target characterization, and biochemical and microbiological validation could further clarify the biological relevance, target-associated activity, and antibacterial potential of L7G against MDR-UPEC.

References:

1. Bernaitis L, Bharathi Priya, Ezhilarasu A, Revathi P, Shenoy RP. Isolation and molecular characterization of multidrug-resistant uropathogenic Escherichia coli from urine samples: Insights into urinary tract infection management. Microbe. 2024. doi:10.1016/j.microb.2024.100185.
2. Medina M, Castillo-Pino E. An introduction to the epidemiology and burden of urinary tract infections. Ther Adv Urol. 2019;11:1756287219832172.
3. Manges AR, Geum HM, Guo A, Edens TJ, Fibke CD, Pitout JDD. Global extraintestinal pathogenic Escherichia coli (ExPEC) lineages. Clin Microbiol Rev 2019;32:e00135-18.
4. Whelan S, Lucey B, Finn K. Uropathogenic Escherichia coli (UPEC)-associated urinary tract infections: The molecular basis for challenges to effective treatment. Microorganisms. 2023;11:2169. doi:10.3390/microorganisms11092169.
5. Loubet P, Ranfaing J, Dinh A, Dunyach-Remy C, Bernard L, Bruyère F, Lavigne JP, Sotto A. Alternative therapeutic options to antibiotics for the treatment of urinary tract infections. Front Microbiol. 2020;11:1509. doi:10.3389/fmicb.2020.01509.
6. Gakuubi MM, Munusamy M, Liang ZX, Ng SB. Fungal endophytes: A promising frontier for discovery of novel bioactive compounds. J Fungi. 2021;7:786. doi:10.3390/jof7100786.
7. Rochín-Hernández LS, Rochín-Hernández LJ, Flores-Cotera LB. Endophytes, a potential source of bioactive compounds to curtail the formation-accumulation of advanced glycation end products: A review. Molecules. 2022;27(14):4469. doi:10.3390/molecules27144469.
8. Kishore KC, Arifullah M, Chakradhar T, Vikram P. In vitro propagation, phytochemical investigations and biological activities of an endemic medicinal plant, Indian red wood (Soymida febrifuga): A review. Int J Med Plants Photon. 2014;107:558-571.
9. Monali M, Sibanarayan R, Shasank SS, Goutam G. In vitro antibacterial activity of crude extracts of nine selected medicinal plants against urinary tract infection-causing multidrug-resistant bacteria. J King Saud Univ Sci. 2017;29(1):84-95. doi:10.1016/j.jksus.2015.05.007.
10. Chandra H, Singh C, Kumari P, Yadav S, Mishra AP, Laishevtcev A, Brisc C, Brisc MC, Munteanu MA, Bungau S. Promising roles of alternative medicine and plant-based nanotechnology as remedies for urinary tract infections. Molecules. 2020;25(23):5593. doi:10.3390/molecules25235593.
11. Bouyahya A, Taha D, Benali T, Zengin G, El Omari N, El Hachlafi N, Khalid A, Abdalla AN, Ardianto C, Tan CS, Ming LC, Sahib N. Natural sources, biological effects, and pharmacological properties of cymaroside. Biomed Pharmacother. 2023;161:114337. doi:10.1016/j.biopha.2023.114337.
12. Chiruvella KK, Mohammed A, Dampuri G, Ghanta RG, Raghavan SC. Phytochemical and antimicrobial studies of methyl angolensate and luteolin-7-O-glucoside isolated from callus cultures of Soymida febrifuga. Int J Biomed Sci. 2007;3(4):269-278. PMID:23675053 PMCID:PMC3614660.
13. Kaur H, Modgil V, Chaudhary N, Mohan B, Taneja N. Computational-guided drug target identification against extended-spectrum β-lactamase-producing multidrug-resistant uropathogenic Escherichia coli. Biomedicines. 2023;11:2028. doi:10.3390/biomedicines11072028.
14. Bouillaut L, Newton W, Sonenshein AL, Belitsky BR. DdlR, an essential

transcriptional regulator of peptidoglycan biosynthesis in Clostridioides difficile. Mol Microbiol. 2019;112(5):1453-1470. doi:10.1111/mmi.14371.
15. Pederick JL, Thompson AP, Bell SG, Bruning JB. D-Alanine-D-alanine ligase as a model for the activation of ATP-grasp enzymes by monovalent cations. J Biol Chem. 2020;295(23):7894-7904. doi:10.1074/jbc.RA120.012936.
16. Acquistapace IM, Thompson EJ, Kühn I, Bedford MR, Brearley CA, Hemmings AM. Insights to the structural basis for the stereospecificity of the Escherichia coli phytase, AppA. International Journal of Molecular Sciences. 2022;23(11):6346. doi:10.3390/ijms23116346.
17. RCSB Protein Data Bank. Available from: https://www.rcsb.org/.
18. Forli S, Huey R, Pique ME, Sanner MF, Goodsell DS, Olson AJ. Computational protein-ligand docking and virtual drug screening with the AutoDock suite. Nat Protoc. 2016;11(5):905-919. doi:10.1038/nprot.2016.051.
19. Bowers KJ, Chow DE, Xu H, Dror RO, Eastwood MP, Gregersen BA, et al. Scalable algorithms for molecular dynamics simulations on commodity clusters. In: Proceedings of the ACM/IEEE Conference on Supercomputing (SC'06). New York: IEEE; 2006. p. 43.
20. Chow E, Rendleman CA, Bowers KJ, Dror RO, Hughes DH, Gullingsrud J, et al. Desmond performance on a cluster of multicore processors. New York: D. E. Shaw Research; 2008. Technical Report No.: DESRES/TR-2008-01.
21. Shivakumar D, Williams J, Wu Y, Damm W, Shelley J, Sherman W. Prediction of absolute solvation free energies using molecular dynamics free energy perturbation and the OPLS force field. J Chem Theory Comput. 2010;6(5):1509-1519. doi:10.1021/ct900587b.
22. Jorgensen WL, Chandrasekhar J, Madura JD, Impey RW, Klein ML. Comparison of simple potential functions for simulating liquid water. J Chem Phys. 1983;79(2):926-935. doi:10.1063/1.445869.
23. Martyna GJ, Tobias DJ, Klein ML. Constant-pressure molecular dynamics algorithms. J Chem Phys. 1994;101:4177-4189. doi:10.1063/1.467468.
24. Martyna GJ, Klein ML, Tuckerman M. Nosé-Hoover chains: The canonical ensemble via continuous dynamics. J Chem Phys. 1992;97:2635-2643. doi:10.1063/1.463940.
25. Toukmaji AY, Board JA. Ewald summation techniques in perspective: A survey. Comput Phys Commun. 1996;95:73-92. doi:10.1016/0010-4655(96)00016-1.
26. Bosshard HR, Marti DN, Jelesarov I. Protein stabilization by salt bridges: Concepts, experimental approaches and clarification of some misunderstandings. J Mol Recognit. 2004;17(1):1-16.
27. SwissADME. Available from: http://www.swissadme.ch/.
28. pkCSM. Available from: http://biosig.unimelb.edu.au/pkcsm/prediction.
29. Kot B. Antibiotic resistance among uropathogenic Escherichia coli. Pol J Microbiol. 2019;68(4):403-415. PMID:31880885 PMCID:PMC7260639. doi:10.33073/pjm-2019-048.
30. Rozwadowski M, Gawel D. Molecular factors and mechanisms driving multidrug resistance in uropathogenic Escherichia coli: An update. Genes (Basel). 2022;13(8):1397. doi:10.3390/genes13081397.
31. Rahman MM, Hossain MMK, Rubaya R, Halder J, Karim ME, Bhuiya AA, Khatun A, Alam J. Association of antibiotic resistance traits in uropathogenic Escherichia coli(UPEC) isolates. Can J Infect Dis Med Microbiol. 2022;2022:4251486. doi:10.1155/2022/4251486.
32. Jayananda IMKI, Ilangakoon ACSI, Kariyakarawanage MKF, Dissanayaka MMKD, Nimna PDR, Lakmini HW, Dineshani H. In vitro antibacterial properties of ten medicinal plants against common uropathogenic organisms and toxicity determination using brine shrimp lethality assay. BMC Complement Med Ther. 2024;24:301.
33. Stanzione F, Giangreco I, Cole JC. Use of molecular docking computational tools in drug discovery. Prog Med Chem. 2021;60:273-343.
34. Bruning JB, Murillo AC, Chacon O, Barletta RG, Sacchettini JC. Structure of the Mycobacterium tuberculosis D-alanine:D-alanine ligase, a target of the antituberculosis drug D-cycloserine. Antimicrob Agents Chemother. 2011;55(1):291-301.
35. Pandeya A, Ojo I, Alegun O, Wei Y. Periplasmic targets for the development of effective antimicrobials against Gram-negative bacteria. ACS Infect Dis. 2020;6(9):2337-2354.
36. Salo-Ahen OMH, Alanko I, Bhadane R, Alexandre A, Honorato RV, Hossain S,

Juffer AH, Kabedev A, Lahtela-Kakkonen M, Larsen AS, et al. Molecular dynamics simulations in drug discovery and pharmaceutical development. Processes. 2021;9(1):71.

37. Wu D, Kong Y, Han C, Chen J, Hu L, Jiang H, Shen X. D-Alanine:D-alanine ligase as a new target for the flavonoids quercetin and apigenin. International Journal of Antimicrobial Agents. 2008;32(5):421–426. doi:10.1016/j.ijantimicag.2008.06.010.
38. Al-Bar OAM, O'Connor CD. Characterization of the D-alanine:D-alanine ligase of Escherichia coli. Biochemical Journal. 1992;282(Pt 3):747–752. https://doi.org/10.1042/bj2820747
39. Zawadzke LE, Bugg TDH, Walsh CT. Existence of two D-alanine:D-alanine ligases in Escherichia coli: cloning and sequencing of the ddlA gene and purification and characterization of the DdlA and DdlB enzymes. Biochemistry. 1991;30(6):1673–1682. https://doi.org/10.1021/bi00220a030